Deciphering human ribonucleoprotein regulatory networks

Neelanjan Mukherjee[1], Hans-Hermann Wessels[2], Svetlana Lebedeva[2], Marcin Sajek[3,4], Mahsa Ghanbari[2], Aitor Garzia[4], Alina Munteanu[2], Thalia Farazi[4*], Jessica I Hoell[4,5], Kemal Akat[4], Thomas Tuschl[4], Uwe Ohler[2]

[1]Department of Biochemistry and Molecular Genetics, University of Colorado School of Medicine, Aurora, Colorado 80045, USA.

[2]Berlin Institute for Medical Systems Biology, Max Delbrück Center for Molecular Medicine, Berlin, Germany.

[3]Institute of Human Genetics, Polish Academy of Sciences, Poznan, Poland

[4]Howard Hughes Medical Institute and Laboratory for RNA Molecular Biology, The Rockefeller University, 1230 York Ave, Box 186, New York, NY 10065

[5]Department of Pediatric Oncology, Hematology and Clinical Immunology, Center for Child and Adolescent Health, Medical Faculty, Heinrich Heine University of Dusseldorf, Dusseldorf, Germany

[*]Current address, Juno Therapeutics, 400 Dexter Avenue North, Seattle, WA 98109

Correspondence to: ttuschl@rockefeller.edu, uwe.ohler@mdc-berlin.de, neelanjan.mukherjee@ucdenver.edu

RNA-binding proteins (RBPs) control and coordinate each stage in the life cycle of RNAs. Although *in vivo* binding sites of RBPs can now be determined genome-wide, most studies typically focused on individual RBPs. Here, we examined a large compendium of 114 high-quality transcriptome-wide *in vivo* RBP-RNA cross-linking interaction datasets generated by the same protocol in the same cell line and representing 64 distinct RBPs. Comparative analysis of categories of target RNA binding preference, sequence preference, and transcript region specificity was performed, and identified potential posttranscriptional regulatory modules, i.e. specific combinations of RBPs that bind to specific sets of RNAs and targeted regions. These regulatory modules encoded functionally related proteins and exhibited distinct differences in RNA metabolism, expression variance, as well as subcellular localization. This integrative investigation of experimental RBP-RNA interaction evidence and RBP regulatory function in a human cell line will be a valuable resource for understanding the complexity of post-transcriptional regulation.

33 **Introduction**

34 Of the 20,345 annotated protein-coding genes in human, at least 1,542 are RNA-binding proteins
35 (RBPs) (Gerstberger et al., 2014). RBPs interact with RNA regulatory elements within RNA
36 targets to control splicing, nuclear export, localization, stability, and translation (Moore, 2005).
37 RBPs have specificity to bind one or multiple RNA categories, including messenger RNA
38 (mRNA) and diverse categories of non-coding RNA such as ribosomal RNA (rRNA), transfer
39 RNA (tRNA), small nuclear and nucleolar RNA (snRNA/snoRNA), microRNA (miRNA), and
40 long non-coding RNA (lncRNA). Mutations in RBPs or RNA regulatory elements can result in
41 defects in RNA metabolism that cause human disease (Cooper et al., 2009; Fredericks et al.,
42 2015).
43
44 A standard technique for *in vivo* global identification of RBP-RNA interaction sites consists of
45 immunoprecipitating the ribonucleoprotein (RNP) complex, isolating the bound RNA, and
46 quantifying the RNA targets by microarrays or deep sequencing (Tenenbaum et al., 2000; Zhao
47 et al., 2010). The introduction of cross-linking prior to immunoprecipitation (CLIP) as well as
48 RNase digestion enabled the biochemical mapping of individual interaction sites (Ule et al.,
49 2003). Subsequent modifications to CLIP increased the resolution of the interaction sites (Hafner
50 et al., 2010; König et al., 2010). One of these methods, photoactivatable ribonucleoside-
51 enhanced cross-linking and immunoprecipitation (PAR-CLIP), utilizes 4-thiouridine or 6-
52 thioguanosine combined with 365 nm UV crosslinking to produce single-nucleotide RBP-RNA
53 interaction evidence that is utilized to define binding sites (Corcoran et al., 2011; Garzia et al.,
54 2017b; Hafner et al., 2010).

55 Experimentally-derived RBP binding sites provide valuable functional insights. First, they can
56 reveal the rules for regulatory site recognition by the RBP, whether due to sequence and/or
57 structural characteristics. Second, the region and position of the interaction sites of an RBP
58 within transcripts provides insights into its role in RNA metabolism and its subcellular
59 localization. For example, if most of the mapped interaction sites are intronic and adjacent to
60 splice sites, the RBP is highly likely to be a nuclear splicing factor rather than a cytoplasmic
61 translation factor. Finally, these data reveal the target transcripts and therefore the potential
62 biological role for the RBP.
63
64 Throughout the life of an RNA, interactions with many different RBPs determine the ultimate
65 fate of the transcript. Even though profiling of the interaction sites of a single RBP is clearly
66 powerful, it does not provide information on other RBPs potentially targeting the same RNA or
67 on other regulatory elements within the RNA. Small comparative efforts focusing on the
68 regulation of splicing, 3' end processing, RNA stability by AU-rich elements, and miRNA-
69 mediated silencing have demonstrated the value of integrating interaction sites from multiple
70 RBPs (Martin et al., 2012; Mukherjee et al., 2014; Pandit et al., 2013; Zhang et al., 2010).
71 Therefore, a large-scale comparative examination of interaction sites for many RBPs will yield
72 valuable knowledge regarding the architecture and determinants of RNA regulatory networks.
73
74 At least 173 PAR-CLIP experiments have been performed in HEK293 cells to date, laying the
75 groundwork for a large-scale integrative analysis and complementing efforts of ENCODE, which
76 focused on other cell types and utilized other CLIP protocols (Van Nostrand et al., 2016). We
77 describe a concerted effort to identify and uniformly process all high-quality PAR-CLIP data sets

78 by evaluating the characteristic T-to-C transitions induced by photocrosslinking. Using the
79 resulting compendium of high-quality in vivo RBP interaction maps from the same cell line
80 enabled us to determine the relationship between RBPs with respect to their preferred category of
81 target RNA and any underlying sequence specificity. We uncovered regulatory modules reflected
82 by combinatorial binding events, and assessed their role and functional implications on RNA
83 metabolism. Finally, our results support the role of RBPs in buffering gene expression variance.
84

85 **Results**

86 **A high-quality map of in vivo RBP-RNA interactions across 64 proteins**

87 In order to generate a comprehensive quantitative resource of RBP-RNA interactions within a
88 human cell line, we identified 166 published PAR-CLIP data sets performed predominantly in
89 HEK293 cells, and added 7 new libraries generated in our laboratories (Sup Table 1). Typically,
90 these datasets were generated using transgenic HEK293 cell lines in which each individual RBP
91 was FLAG-tagged and recombined into the same chromosomal locus containing a strong
92 promoter. In this way, the expression of each RBP as well as the strength of its
93 immunoprecipitation were generally comparable. Furthermore, the availability of orthogonal
94 transcriptome-wide datasets quantifying individual steps of RNA metabolism made HEK293
95 cells ideal for examining the functional characteristics of RNA targets (Mukherjee et al., 2017).

96

97 Each of the 173 PAR-CLIP libraries generated in HEK293 were subject to a stringent analysis
98 strategy to retain high-quality datasets (Supplemental Table 1). First, each library was analyzed
99 using the PAR-CLIP Suite v1.0 (https://rnaworld.rockefeller.edu/PARCLIP_suite) (Garzia et al.,

100 2017b) to discriminate significant target RNA categories from non-crosslinked background RNA
101 categories populated by fragments of abundant cellular RNAs (see Methods, Supplemental Fig.
102 1A). Next, we defined binding sites based on the local density of T-to-C transitions using
103 PARpipe (https://github.com/ohlerlab/PARpipe) (Corcoran et al., 2011) and only retained those
104 libraries with sufficiently high read counts and T-to-C transition specificity compared to a deeply
105 sequenced background reference library (Supplemental Fig 1b) (Friedersdorf and Keene, 2014).
106 Since the immunoprecipitation step was omitted in this reference library it served as an effective
107 comparison point to score read count and T-to-C transition for all RBPs. Finally, for RBPs with
108 more than 3 libraries available, outlier libraries exhibiting poor correlation of 6-mer frequencies
109 were excluded (Supplemental Fig 1d, e). This resulted in 114 libraries corresponding to 64 RBPs
110 that were the basis for downstream analysis. There were eight RBP families represented by two
111 or more RBPs.

112

113 **Grouping RBPs by annotation category and positional binding site preferences**

114 As first step to describe RBP-RNA regulatory networks, we determined the relative binding
115 preference of each RBP for specific target RNA annotation categories (Supplemental Table 2).
116 For each library, we calculated an RNA annotation category preference value, defined as the
117 difference in the fraction of T-to-C reads per annotation category between each RBP library and
118 the reference library. We performed hierarchical clustering of RBPs by annotation category
119 preference, using Ward's method and Euclidean distances. This yielded eight clusters of binding
120 preference (Figure 1a – orange line demarcates cluster definitions) with varying enrichment or
121 depletion for individual or combinations of specific annotation categories. For each of these
122 clusters, we compiled a detailed table summarizing the reported functions for each of the RBPs

123 (Table 1). Taken together, clustering by RNA annotation category separated RBPs into groups
124 according to their known subcellular localization and functions.

125 Three of the eight clusters (clusters 2, 4, and 5) contained nine RBPs that exhibited preference
126 for categories of non-coding RNA (rRNA, snRNA, snoRNA, and tRNA), but not mRNA,
127 precursor mRNA (pre-mRNA), or lncRNA. The remaining five clusters contained 55 RBPs
128 exhibiting preference for binding to mRNA, pre-mRNA and long-noncoding RNA (lncRNA)
129 annotation categories. The RBPs in clusters 1, 6, 7, and 8 exhibited strong preferences for
130 various mRNA annotation categories. The RBPs in cluster 3 did not exhibiting strong preference
131 for specific mRNA annotation categories. Additionally, for each of the RBPs in the cluster, we
132 performed a positional meta-analysis of binding sites with respect to major transcript landmarks
133 within target mRNAs. Many of the RBPs also showed strong preferences for binding to specific
134 positions within mRNAs relating to their role in specific steps of mRNA processing (Table 1).

135 We hypothesized that target annotation category preferences and positional binding preferences
136 should reflect subcellular localization of the RBP and its role(s) in mRNA processing. Cluster 6
137 contained twelve RBPs and exhibited strong preference for intronic regions and to a lesser
138 degree 3' UTRs of mRNAs and lncRNAs. The intronic preference was consistent with the
139 predominantly nuclear localization of these RBPs and the pre-mRNA splicing process. ELAVL1,
140 which is the sole member of the ELAVL1 family of RBPs that is predominantly localized in the
141 nucleus but capable of shuttling to the cytoplasm, exhibited positional binding flanking the end
142 of the 3' UTR and for 5' and 3' splice sites. Cluster 8 contained fourteen RBPs and exhibited
143 distinct preference for 3' UTR regions. This included the unpublished and predominantly
144 cytoplasmic ELAVL1 family members, ELAVL2, ELAVL3, and ELAVL4, which exhibited a
145 strong positional preference for binding in the distal region of the 3' UTR and acting

146 predominantly on mature mRNA (Mansfield and Keene, 2012). In summary, the annotation
147 category preferences and positional binding preferences implicated the specific steps of mRNA
148 processing the RBPs potentially regulate.

149

150 **The spectrum of RNA sequence specificity**

151 RBPs exist on a spectrum of specificity depending on a variety of primary and secondary
152 structure features (Jankowsky and Harris, 2015). Here, our goal was to identify the RBPs with
153 substantial primary sequence specificity and then examine their sequence preference. For each of
154 the 55 RBPs, we counted all possible 6-mers using Jellyfish (Marçais and Kingsford, 2011) for
155 the reads contributing to PARalyzer-defined binding sites. We observed 6-mer frequencies
156 ranging as high as 512-fold to as low as 5-fold over a uniform distribution of 6-mers
157 (Supplemental figure 2a). In contrast, our reference background library exhibited 16-fold
158 enrichment of at least one 6-mer compared to uniform. AGO1-4 libraries were excluded from 6-
159 mer analysis due to the overwhelming sequence contribution from crosslinked miRNAs. Twenty-
160 seven RBPs did not have a single 6-mer found at higher frequency than present in the reference
161 sample. Amongst these RBPs established or expected to display low sequence-specificity were
162 the RNA helicase MOV10, the nuclear exosome component DIS3, and the EIF3 complex
163 translation initiation factors.

164

165 For each of the 24 RBPs with stronger sequence enrichment than the reference library, we
166 clustered the top 5 sequences enriched over the reference library (Figure 2). Our results
167 recapitulated the sequence preference for the RBPs in this group with well-characterized
168 sequence motifs (detailed in Table 2). The ELAVL1 family proteins, which bound to different

169 regions and positions of mRNA, showed similar preference for U- and AU-rich 6-mers, while
170 ZFP36 only enriched a subset of the AU-rich 6-mers (Mukherjee et al., 2014). Complementing
171 the 6-mer enrichment analysis, we performed motif analysis for each RBP library with the motif
172 finding algorithm SSMART (sequence-structure motif identification for RNA-binding
173 proteins, (Munteanu et al., 2018)) (Supplemental Fig 2b). For most RBPs, we observed strong
174 concordance between the two analyses. RBM20 was a clear exception, for which we observed
175 the established UCUU-containing motifs (Maatz et al., 2014) with SSMART, but a GA-rich
176 sequence in the 6-mer enrichment analysis. However, we do observe UCUU-containing motifs in
177 the top 15, but not top5 6-mers for RBM20. Altogether, our analysis was remarkably consistent
178 with previously reported motifs in spite of differences in data processing and analysis (detailed
179 Table 2).

180

181 **Identification of RNA regulatory modules**

182 To understand the functional impact of co-regulation by multiple RBPs, we analyzed the co-
183 variation in binding patterns of all 55 RBPs across 13,299 target RNA encoding genes to probe
184 for the existence of regulatory modules, i.e., specific subsets of RNAs implicated in similar
185 function bound by subsets of RBPs. To this end, we employed Factor Analysis (FA), which
186 reduces a large number of observed variables to a smaller number of latent *factors*. Here, our
187 observed variables represented the normalized RBP binding (see methods) for each of the 55
188 RBPs across all target RNA encoding genes (n=13,299). The latent *factors* represented similar
189 binding patterns to RNA targets by one or more of the 55 RBPs. RBPs exhibiting high loadings
190 for the same *factor* would have very similar binding patterns to RNA targets. Importantly in this

191 framework, a single RBP could be assigned to multiple *factors*, just as a single RBP can
192 participate in multiple RNPs and regulate different aspects of RNA metabolism.
193
194 The FA model decomposed the 55 x 13,299 normalized RBP binding matrix into a 55 x 10 factor
195 loading matrix (representing the strength of the dependence of each of the 55 RBP target RNA
196 binding pattern on each of the 10 *factors*), a 13,299 x 10 factor score coefficient matrix
197 (representing the dependence between the binding of the 13,299 target RNA encoding gene and
198 each of the 10 *factors*), and residual error (Supplemental Fig 3a and methods). Cumulatively, the
199 FA model explained ~60% of the variance in the observed data. The remaining unexplained
200 variance was expected due to the challenges of integrating data sets of varying depth and quality,
201 in spite of our efforts to control these aspects. The communality, which is the amount of variance
202 explained by the model for each RBP-binding variable, varied drastically for all 55 RBPs; the
203 model explained at least 80% of the variance in enrichment scores for 12 RBPs, and at least 50%
204 of the variance in enrichment scores for 30 RBPs (Supplemental Figure 3b). RBPs with lower
205 communality often coincided with shallow depth of their PAR-CLIP libraries.
206
207 The FA model also uncovered interesting parallels between the similarity in the binding of target
208 RNA encoding genes and the target annotation category preferences (from Figure 1a). We
209 observed that individual *factors* contained RBPs that preferred binding to either mature (Factors
210 1, 3, 4, 5, 8) or precursor transcripts (Factors 2, 6), reflecting involvement in different stages of
211 RNA metabolism (Figure 3a). Furthermore, individual *factors* contained RBPs exhibiting similar
212 patterns of binding to specific regions of the mRNA (i.e., intron, coding, 3' UTR). Indeed, RBPs
213 from the same family, or known to regulate a specific aspect of RNA processing, had high

214 loadings for the same *factors*. For example, the ELAVL1 family members were associated with
215 Factor 1; the AGO1 family were associated with Factor 3; the IGF2BP1 family were associated
216 with Factor 4; the FMR1 family had were associated with Factor 5 and Factor 8; LINE-1
217 encoded proteins were associated with Factor 7. One of the unanticipated associations was that
218 of HNRNPC with Factor 2, which contained mainly cleavage and polyadenylation factors.
219 Interestingly, HNRNPC was shown to interact with U-rich sequences downstream of a viral
220 poly-adenylation signal nearly three decades ago (Wilusz et al., 1988), and more recently, to
221 repress cleavage and poly-adenylation in humans (Gruber et al., 2016). These examples highlight
222 the specific testable hypotheses generated by an integrative analysis that are not necessarily
223 obvious when examining a single RBP in isolation.
224
225 By clustering the factor score coefficients, i.e. the specific linear combination of RBP binding for
226 that target RNA, we identified target RNA encoding genes constituting putative regulatory
227 modules associated with a given *factor*. Therefore, each regulatory module was associated with
228 an RBP component (the subset of RBPs exhibiting similar binding pattern) and a RNA
229 component (the subsets of target RNA encoding genes bound by those RBPs). These regulatory
230 modules did not imply physical interactions between RBPs; rather, it identified RBPs that may
231 cooperate in controlling RNA metabolism for specific subsets of RNA targets, possibly across
232 cellular compartments. Almost a quarter of the target RNA encoding genes (3,180/13,299) were
233 assigned to regulatory modules by exhibiting high factor score coefficients for a single *factor*
234 (Supplemental figure 3c). We did not identify target RNA encoding genes with high factor score
235 coefficients for Factor 9 or 10. The remaining target RNA encoding genes did not exhibit high
236 factor score coefficients for any specific *factor* in our analysis, suggesting that the targets were

237 either not bound by specific combinations of these RBPs, bound broadly by all RBPs, or not
238 bound by the subset of RBPs in the analysis. As such, we labeled this target RNA encoding gene
239 category as "non-specific". The RNA regulatory modules encoding genes were enriched for
240 different GO categories. Factor 1 RNA regulatory modules were enriched for 'AU-rich element
241 binding' and Factor 3 RNA regulatory modules were enriched for 'gene silencing by miRNA';
242 AU-rich RBPs and AGO proteins were strongly associated with Factor 1 and Factor 3,
243 respectively. This was consistent with the recurrent observation that RBPs target the mRNAs
244 encoding themselves (Pullmann et al., 2007; Tenenbaum et al., 2000). In turn, the RNAs
245 encoding "non-specific" genes contained ribosomal proteins and mitochondrial electron-
246 transport proteins.
247

248 **RNA regulatory modules underlie distinct patterns of RNA metabolism**

249 In order to test the functional relevance of these RNA regulatory modules, we reasoned that
250 perturbation (change of protein abundance or activity) of an RBP will lead to pronounced effects
251 only for the RNA regulatory modules assigned to the specific *factor(s)* that RBP is associated
252 with. We examined mature and precursor RNA expression changes induced by siRNA
253 knockdown of ELAVL1 (Kishore et al., 2011). ELAVL1 was strongly associated with both
254 Factor 1 and Factor 2, which exhibited RNA targeting patterns for mature or precursor RNAs,
255 respectively. Concordantly, Factor 1 associated RNA regulatory modules, but not Factor 2 RNA
256 regulatory modules, exhibited ELAVL1-dependent stabilization of mature RNA (Figure 4a).
257 Likewise, Factor 2 RNA regulatory modules exhibited a more pronounced ELAVL1-dependent
258 stabilization of precursor RNA than Factor 1 RNA regulatory modules (Figure 4b). Each human
259 ELAV1 family protein contains three RRM domains (>90% sequence identity), but the hinge

260 region between the second and third RRM of ELAVL1 contains a shuttling sequence responsible
261 for its nuclear localization (Fan and Steitz, 1998). Due to the lack of this shuttling sequence,
262 ELAVL2/3/4 are predominantly cytoplasmic and were strongly associated with Factor 1, but not
263 Factor 2. Taken together, the model was able to correctly identify and distinguish ELAVL1-
264 dependent stabilization of both precursor and mature RNA (Lebedeva et al., 2011; Mukherjee et
265 al., 2011).
266
267 We hypothesized that the subsets of RNAs assigned to the different regulatory module would
268 exhibit differences in RNA metabolism driven by the RBPs in the *factor* associated with the
269 regulatory module. Therefore, we compared six aspects of RNA metabolism previously
270 quantified in HEK293 cells (Mukherjee et al., 2017), for each of the RNA regulatory modules
271 associated with each of the *factors*. The *factor*-associated RNA regulatory modules exhibited
272 very distinct RNA metabolic profiles compared to each other and to non-specific category
273 (Figure 4c, Supplemental Figure 4a). Factor 2 RNA regulatory modules, which was the only
274 factor associated with RBPs binding to precursor mRNA and lncRNA, had low processing rates,
275 high degradation rates and their encoded RNAs were preferentially localized in the nucleus
276 versus the cytoplasm. Factor 2 RNA regulatory modules were strongly enriched for lncRNAs
277 (Figure 4d). Indeed, these genes strongly overlapped with a set of lncRNAs likely to be
278 functional (Supplemental figure 4b) (Mukherjee et al., 2017).
279
280 We also examined regulatory differences in RNA metabolism for genes associated with
281 cytoplasm-enriched factors. For example, factor 1 RNA regulatory modules were more stable
282 than Factor 3 RNA regulatory modules (Figure 4c). Factor 1 was strongly associated with

283 ELAVL1 family proteins, which stabilize target mRNAs. Factor 3 was strongly associated with
284 AGO1 family proteins, which execute miRNA-mediated degradation of target mRNAs.
285 Additionally, Factor 4 RNA regulatory modules, which are bound by IGF2BP1 family proteins,
286 were highly synthesized, processed, stabilized, and translated (Figure 4c). The RNA targets of
287 IGF2BP1 family RBPs were strongly localized to the ER (Supplemental Figure 4c) (Jønson et
288 al., 2007), which is also consistent with the proposed role of IGF2BP1 family proteins for RNA
289 localization and translation (Farina et al., 2003; Nielsen et al., 2001). Although correlative, these
290 results indicate that different RBP binding patterns beget different consequences for RNA
291 metabolism.
292
293 Specific RNA regulatory modules also exhibited preferential localization to processing bodies
294 (P-bodies), which are cytoplasmic granules associated with translational repression (Sheth and
295 Parker, 2003). Namely, Factor 3 RNA regulatory modules, which were strongly associated with
296 the AGO1 family, were the most strongly enriched for localizing to P-bodies according to a
297 recent study characterizing the transcriptome and proteome of P-bodies, and the AGO2 protein
298 itself was 90-fold enriched (Hubstenberger et al., 2017). Similarly, Factor 5 RNA regulatory
299 modules, which were strongly associated with the FMR1 family, were also enriched for
300 localizing in P-bodies, along with the FMR1 protein (16-fold enriched). In contrast, the non-
301 specific category was depleted from P-bodies.
302
303 Fine-tuning of gene expression has been postulated to be an important function of post-
304 transcriptional regulation by RBP and miRNAs. Therefore, we examined the cell-to-cell
305 variability in gene expression across 25 individual HEK293 cells with respect to the RNA

306 regulatory modules. The single-cell RNA-seq data was very deeply sequenced and generated
307 using the massively parallel single-cell RNA-sequencing (MARS-Seq) protocol (Guillaumet-
308 Adkins et al., 2017). Most RNA regulatory modules exhibited lower expression variability than
309 the non-specific category (Figure 4e). In particular, Factor 4 RNA regulatory modules exhibited
310 the lowest variation and highest median expression across the 25 cells (Supplemental Figure 4d).
311 These results supported the broad notion that post-transcriptional gene regulation generally
312 confers robustness and fine-tuning of gene expression.
313
314 **Conclusion**

315 Our study presents a curation of existing datasets, followed by systematic analysis of high-
316 quality and high-resolution RBP-RNA interaction data. We focused on the RBPs that
317 preferentially bound to mRNA and lncRNA and examined their sequence specificity and
318 sequence motif preferences. Our survey of the RBP regulatory landscape identified the most
319 prevalent subsets of RNAs targeted by a specific subset of RBPs, which we refer to as RNA
320 regulatory modules.
321
322 We utilized high quality PAR-CLIP datasets for which the immunoprecipitation was generally
323 comparable due to fact most RBPs were FLAG-tagged. Nevertheless, several caveats associated
324 with the interpretation of this analysis need to be pointed out. Despite several measures of quality
325 control to decide which datasets to include in our analysis, the libraries varied greatly in depth,
326 quality, digestion biases and potentially other confounding variables with respect to the protocol.
327 The FA model quantitatively assessed the degree to which we could explain the full complement
328 of RBP-RNA target binding patterns. These confounders undoubtedly contributed to the ~40%

329 of variance not explained by the FA model. In comparison, the ENCODE eCLIP datasets (Van
330 Nostrand et al., 2016) are likely to suffer from different confounders: they were generated using
331 one consistent experimental protocol but used antibodies against endogenous proteins expressed
332 at varying levels, and for which IP efficiency can vary greatly in spite of the quality control
333 performed (Sundararaman et al., 2016). Essentially, this represents the trade-offs in experimental
334 design between analyzing the endogenous protein compared to an epitope-tagged protein.
335 Modifying the genomic loci of the protein to engineer an endogenous epitope tagged RBP is
336 a very promising strategy.
337
338 Assuming the RBPs investigated here are a representative sample of the ~1,542 RBPs encoded in
339 the human genome, there may be an astounding number of RBPs with substantial primary
340 sequence specificity. However, the degree of sequence specificity is determined by the nature of
341 the RBP-RNA interaction, which can be quite extensive and specific, as in the case of Pumilio,
342 or minimal and non-sequence specific, as in the case of an RNA-helicase. An interesting
343 exception were the A-rich sequences enriched by UPF1, which is an RNA helicase and therefore
344 unlikely to exhibit strong sequence specificity. One possible explanation is that such sequences
345 may represent pre-mature polyA tail recognition involved in aspects of ribosome quality control
346 demonstrated in yeast (Koutmou et al., 2015) and human cells (Garzia et al., 2017a). Likewise,
347 more examples of unanticipated sequence enrichments may shed light on novel RNA regulatory
348 mechanisms.
349
350 Our FA model was able to identify distinct RBP-RNA target regulatory modules. At the very
351 minimum, 25% of target RNA encoding genes were assigned to RNA regulatory modules. This

352 is very likely an underestimation due to noisy data and a biased, far from complete sampling of
353 RBPs. However, there is likely to be a subset of genes for which post-transcriptional gene
354 regulation indeed plays a negligible role, at least in HEK293 cells. Furthermore, a small number
355 of RBPs in our analysis are not endogenously expressed in HEK293 and their natural expression
356 is tissue-specific and/or context-dependent. The approach presented here can scale to binding
357 data for all ~700 RBPs experimentally shown to be associated with poly-adenylated RNA in
358 HEK293 cells or even ~1,542 known RBPs (Baltz et al., 2012).
359
360 The RNA regulatory modules exhibited different patterns of RNA processing, degradation,
361 localization, and translation. We speculate that these differences in RNA metabolism were driven
362 by individual RBPs or the combination of RBPs associated with that regulatory module. This
363 was supported by the response of specific RNA regulatory modules to ELAVL1 knockdown
364 (Figure 4A, B). Additionally, the RNA regulatory modules encoded functionally related proteins
365 and similarly localized proteins. The enrichments were for proteins with similar molecular
366 functions or multi-component complexes rather than signaling pathways (Supplemental Fig 3b).
367 Altogether, these lines of evidence provide support for the coordinate regulation of 'functionally
368 coherent' RNA regulatory modules as proposed by the post-transcriptional operon/regulon model
369 (Keene, 2007). The ultimate test of this model would involve manipulating specific combinations
370 of binding sites and RBPs. Our study provides the rationale for such experiments, which
371 unfortunately remain technically challenging.
372
373 Our observations have important implications for RBP-RNA regulatory networks and their
374 importance in gene expression. The mRNA targets within specific regulatory modules encoded

375 the RBP themselves, a generalization of a commonly made observation that RBPs bind to the
376 mRNAs encoding them (Mesarovic et al., 2004). Our analysis lends support for this frequently
377 observed potential auto-regulatory feedback. These feedback loops may in fact buffer the
378 expression range of the targeted mRNAs, including those of the RBP. In this context, the
379 observation that the RNA regulatory modules exhibited lower cell-to-cell gene expression
380 variance, provides more evidence for the importance of post-transcriptional regulation in
381 buffering transcriptional noise (Bahar Halpern et al., 2015; Battich et al., 2015). Systematic
382 perturbation of individual and combinations of RBPs will be quite powerful in revealing
383 fundamental properties of RNA regulatory networks such as auto-regulatory feedback and
384 buffering.
385
386 The binding preference and targets of the vast majority of human RBPs remains unknown. The
387 insights gained from this study demonstrate the value of large-scale efforts by ENCODE and
388 others in the community to globally identify RBP binding sites. Of the 64 RBPs in this study, 44
389 were not represented in the ENCODE cell lines. Cumulatively these efforts interrogate ~10% of
390 human RBPs with known RNA-binding domains. Thus, these two large scale efforts offer the
391 potential to complement one another in our continuing attempts to understanding RBP-RNA
392 regulatory networks, for which we have only glimpsed the tip of the iceberg.
393
394 **Methods**

395 **Processing, filtering, and quality control of PAR-CLIP libraries**

396 Each PAR-CLIP library was subject to two rounds of quality control. First, all PAR-CLIP
397 libraries generated in HEK293 cells were subject to the quality control pipeline PAR-CLIP Suite

398 v1.0 (https://rnaworld.rockefeller.edu/PARCLIP_suite/). Using raw Illumina sequencing data,
399 this pipeline identified the predominant target RNA category or categories for each RBP and
400 provided the T-to-C conversion frequency resolved by read length and RNA category
401 (Supplemental Fig 1). The mapped reads of each RNA category were resolved by error distance
402 0 (d0), error distance 1 (d1; split in T-to-C and d1 other than T-to-C), and error distance 2 (d2).
403 This process discriminated for each library true target RNA categories from non-crosslinked
404 background RNA categories populated by fragments of abundant cellular RNAs. In order to
405 disqualify experiments comprising too many non-crosslinked RBP-specifically bound RNAs or
406 co-purified non-crosslinked background RNAs, we pursued only datasets which collect at least
407 10,000 redundant d1 reads ≥ 20 nt in at least one of major RNA annotation categories with d1(T-
408 to-C)/(d0 + d1) ≥ 30%, and d1(T-to-C)/(d1-total) ≥ 65%.

409 For the libraries passing the first threshold, we defined and annotated binding sites using
410 PARpipe, which is a pipeline wrapper for PARalyzer (Corcoran et al., 2011; Mukherjee et al.,
411 2014). The threshold for additional filtering were determined by comparisons with the reference
412 library (Friedersdorf and Keene, 2014). This reference library was generated using a modified
413 PAR-CLIP protocol in which there was no immunoprecipitation and the addition of an rRNA
414 depletion step after proteinase K digestion, followed by a partial digestion using RNase T1. We
415 required libraries had to have an average fraction T-to-C over remaining reads greater than 0.32
416 (the average fraction T-to-C over remaining reads greater of the reference library), an average
417 conversion specificity greater than 0, more than 20000 aligned reads, not be digested only with
418 micrococcal nuclease, a redundant read copy fraction less than .98 (Supplemental Fig 1b,c and
419 Sup Table 1). For RBPs with three or more libraries, we removed outlier based on correlation of
420 6-mer frequency calculated from PARalyzer-utilized reads.

421

422 **Annotation category preference and positional analysis of binding density**

423 For calculating the annotation category preference, we calculated the difference in the fraction of
424 T-to-C reads per annotation category between each RBP library and the reference library. For
425 example, if the fraction of miRNA annotated reads with T-to-C transitions in a specific RBP
426 library was 0.20 compared to 0.05 in the reference library, the miRNA preference value for this
427 specific RBP is 0.15. For the positional binding analysis, we selected genes (n=15120) using
428 GENCODE v19 as annotation based on our earlier work on HEK293 RNA processing and
429 turnover dynamics (Mukherjee et al., 2017). Isoform expression was calculated using RSEM (Li
430 and Dewey, 2011). For each gene, we selected the transcript isoform with the highest isoform
431 percentage or chose one randomly in case of ties (n=8298). The list of selected transcript
432 isoforms was used to calculate the median 5' UTR, CDS and 3' UTR length proportions (5'
433 UTR=0.06, CDS=0.53, 3' UTR=0.41) using R Bioconductor packages GenomicFeatures and
434 GenomicRanges. For regions downstream annotated transcription ends (TES) and adjacent to
435 splice sites, we chose windows of fixed sizes (TES 500nt, 5’ and 3’ splice sites 250nt each). We
436 generated coverage tracks from the PARalyzer output alignment files and intersected those with
437 the filtered transcripts. Each annotation category was binned according to its relative coverage
438 averaged according to each bin. For intronic coverage, we averaged across all introns per gene,
439 given a minimal intron length of 500nt. All bins were stitched to one continuous track per
440 transcript. Altogether 6632 intron containing transcripts showed coverage in at least one
441 PARCLIP library. For each library, we required transcripts to have a minimal coverage
442 maximum of > 2. For each transcript, we scaled the binned coverage dividing by its maximal
443 coverage (min-to-1 scaling) to emphasize spatial patterns independent from transcript expression

444 levels. Replicate RBP PARCLIP libraries were combined at this point. Transcripts targeted in
445 more than one replicate library were aggregated using the average of their binned coverage.
446 RBPs with less than 50 filtered target transcripts (after aggregation) were not considered. Next,
447 we split transcript coverage in two parts, separating 5' UTR to TES regions and intronic regions.
448 To generate the scaled meta coverage across all targeted transcripts per RBP, we used the
449 heatMeta function from the Genomation package. For the 5'UTR to TES, we scaled each RBP
450 meta-coverage track independent of other RBPs. For each RBP, we subtracted the scaled meta
451 coverage of PARCLIP reference library (Friedersdorf and Keene, 2014). For intronic sequences,
452 we scaled each RBP relative to all other RBPs to highlight RBPs with more substantial intronic
453 binding patterns. Finally, we visualized the density using pheatmap.
454

455 **Sequence analysis**

456 We calculated 6-mer frequencies with Jellyfish from all reads that generated a PARalyzer
457 binding site for each library. For each RBP, we selected the library with the lowest percent of
458 duplicated sequences (see supplemental table 1) to serve as a representative library for the
459 sequence analysis and factor analysis. For each RBP, we counted the number of 6-mers with a
460 frequency of x or higher, where x was from 1/4096 to 1/4. To evaluate the 6-mers enriched by a
461 given RBP relative to the reference library, we regressed the RBP 6-mer frequency against the
462 the reference library 6-mer frequency and collected the residuals (the unexplained variance).
463 Next, identified all 6-mers that were found as the top 5 enriched over the reference library for
464 any of the analyzed RBPs. We clustered the enrichment scores for the 6-mers across all RBPs
465 and generated a heatmap using the 'aheatmap' function in NMF R package. We ran SSMART

466 using all binding sites found in mRNA-derived annotation categories ranked by the library size
467 normalized enrichment over the reference library.

468 **Factor analysis**

469 For each site identified we calculated a library size normalized enrichment compared to the the
470 reference library. We calculated the sum of all enrichment scores for all sites annotated as
471 mRNA and lncRNA. Next, we normalized for expression levels (collected the residuals) to
472 create the final matrix of values. The number of factors, 10, was determined using the majority
473 result of numerous methods to estimate the number of factors. Clustering of the score matrix was
474 performed using the most stable results from numerous iterations of k-means clustering.

475

476 **Gene ontology analysis**

477 Multiple-test corrected gene ontology enrichment values were calculated using the TOPGO R
478 package. For each set of genes, we used all 13,299 genes in the factor analysis as the background
479 or gene universe. Enrichment was calculated using the 'parent-child' approach on the top 100
480 enriched terms. This metric accounts for the hierarchical organization of gene ontology terms to
481 minimize false-positive enrichments. We performed a Bonferonni multiple test correction on the
482 enrichment p-values.

483

484 **Premature and mature RNA quantification**

485 Mature- and premature-transcript expression, transcripts per million (TPM), was quantified with
486 RSEMv1.2.11 (http://deweylab.biostat.wisc.edu/rsem/src/rsem-1.2.11.tar.gz) as described
487 previously (Mukherjee et al., 2017). Briefly, for each gene we included an additional isoform

488 corresponding to the sequence of the full gene locus. Specifically, we modified the
489 GENCODEv19 gtf and used this as the input for the 'rsem-prepare-reference' function to
490 generate a modified index used for quantification. For each gene, we calculated the expression of
491 'mature' RNA as the sum of all isoforms for that gene excluding the 'primary' transcript. For
492 intronless genes, premature and mature expression values were summed. We performed this
493 analysis on the ELAVL1 knockdown RNA-seq experiments (Kishore et al., 2011).
494

495 **Cell-to-cell expression variability**

496 RNA-seq gene expression data for 25 individual HEK293 cells were downloaded from
497 (Guillaumet-Adkins et al., 2017). We calculated the coefficient of variation (100*standard
498 deviation/mean) for each gene across all 25 cells.

499 **Figure Legends**

500 **Figure 1. RBP analyzed and binding preferences by RNA category.** A) Heatmap of reference
501 normalized annotation category preference for each RBP clustered into 8 branches by color
502 (left). The heatmap represents the difference in the proportion of sites for a given annotation
503 category in the RBP library versus the reference library. Heatmap of the reference library
504 normalized relative positional binding preference of the 55 RBPs with enriched binding in at
505 least one mRNA-relevant annotation category per branch (right). RBP-specific binding
506 preferences were averaged across selected transcripts (see methods). The relative spatial
507 proportion of 5'UTR, coding regions and 3'UTR were averaged across all selected transcript
508 isoforms. For TES (regions beyond transcription end site), 5' splice site, and 3' splice site, we
509 chose fixed windows (250nt for TES and 500nt for splice sites). For each RBP, meta-coverage
510 was scaled between 5'UTR to TES. The 5' and 3' intronic splice site coverage was scaled
511 separately from other regions but relative to each other.

512

513 **Figure 2. RBP binding sequence specificity and elements.** A) Heatmap of reference
514 normalized 6-mer enrichment for top 5 enriched 6-mers for each RBP in the set of RBPs
515 exhibiting more sequence specificity than the reference.

516

517 **Figure 3. RNA regulatory modules.** A) Factor analysis of target RNA encoding genes binding
518 normalized by the reference library and expression for the 55 RBPs binding to mRNAs and
519 lncRNAs for 13,299 genes (see 'factor analysis' section in methods for details). Spring-
520 embedded graph of the factor loading matrix, indicating the association between each of the 55
521 RBPs and one of the 10 factors. Nodes color-coded by RNA annotation category preference

522 cluster membership from figure 1. Edge width scales with factor loadings (thicker edge = higher
523 factor loading = stronger association). Only edges with a factor loading > 0.2 (positive values in
524 black) or < -.2 (negative values in green) depicted.
525
526 **Figure 4. Functional characterization of RNA regulatory modules.** A) The difference in
527 either A) primary or B) mature RNA expression (transcripts per million) upon ELAVL1
528 knockdown by siRNA treatment (y-axis), specifically the $\log_2$[siRNA EGFP TPM]-$\log_2$[siRNA
529 ELAVL1 TPM], for each gene set. C) Heatmap of the median value of synthesis rate, processing
530 rates, degradation rates, cytoplasmic versus nuclear localization, polyribosomal versus
531 cytoplasmic localization, and translational status from ribosome profiling data for each gene set
532 (top). Heatmap of the odds-ratio of the overlap between factor associated gene sets with
533 annotation (bottom). D) Box-and-whisker plot for each gene set of the enrichment in P-bodies.
534 E) Box-and-whisker plot for each gene set of the coefficient of variation across 25 individual
535 HEK293 cells.
536
537 **Supplemental Figure 1. QC filtering of libraries.** A) Description of PAR-CLIP suite to assess
538 library quality control per annotation category (left). Example of number of reads mapping to
539 each RNA category with up to 2 mismatches resolved by length of adapter-extracted sequence
540 reads for an ELAVL1 library (middle). Sequencing read composition of the most abundant RNA
541 category fir the ELAVL1 library. Reads were assigned as d0 (white), d1 T-to-C (red), d1 other
542 than T-to-C, (light gray), and d2 (black) (right). B) Libraries had to have > 20,000 aligned reads
543 and a mean conversion specificity > 0, and a higher mean T-to-C fraction than the the reference
544 library (red lower, blue higher). C) Number of libraries analyzed and their quality control status.

545 D) Count of libraries passing QC per RBP. E) Examples of outlier library removal (libraries
546 labeled with red text were removed) based on correlation of read 6-mer frequency for RBPs with
547 3 or more libraries.
548
549 **Supplemental Figure 2. Grouping RBPs by sequence specificity.** A) Heatmap of the number
550 of 6-mers enriched per RBP at different specificity thresholds. The color scale represents the $\log_2$
551 [number of 6-mers] that are enriched at a given threshold (y-axis). The thresholds are represented
552 as $\log_2$ [6-mer frequency]. There are 4096 different 6-mers and if they were uniformly present
553 this would represent a value of -12 $=\log_2$ [1/4096]. The horizontal dashed lines at -8, represents
554 16-fold enrichment over a uniform background. For reference, the vertical dashed lines indicate
555 the behavior of the reference library. B) Top 3 SSMART motif results using all binding sites
556 found in mRNA-derived annotation categories ranked by the library size normalized enrichment
557 over reference library.
558
559 **Supplemental Figure 3. Factor analysis model selection and performance.** A) Plot
560 of eigenvalues versus number of factors to determine the optimal number of factors using four
561 methods (different colors). B) Barplot of the communality, or the variance in a given RBP
562 cumulatively explained by the all factors. C) Heatmap of the median factor score coefficient
563 value for all genes that clustered together. The number of genes assigned to a specific factor and
564 the top two most significant enriched GO annotations for each ontology class: molecular
565 function (MF), cellular component (CC), and biological process (BP).
566
567

568 **Supplemental Figure 4. RNA metabolism profiles for factor-associated gene sets.** A) Box-
569 and-whisker plot for each gene set of the synthesis rates, processing rates, degradation rates,
570 cytoplasmic versus nuclear localization (Cyt vs Nuc), polyribosomal versus cytoplasmic
571 localization (Poly vs Cyt), and translational status from ribosome profiling data. B) Heatmap of
572 the odds-ratio of the overlap between factor associated gene sets with RNA categories based on
573 similar metabolic profiles from (Mukherjee et al., 2017). C) Heatmap of the odds-ratio of the
574 overlap between factor associated gene sets and protein localization annotation. D) Box-and-
575 whisker plot for each gene set of the median expression across 25 HEK293 cells.

576

577

578 Bahar Halpern, K., Caspi, I., Lemze, D., Levy, M., Landen, S., Elinav, E., Ulitsky, I., Itzkovitz,
579 S., 2015. Nuclear Retention of mRNA in Mammalian Tissues. Cell Rep 13, 2653–2662.
580 doi:10.1016/j.celrep.2015.11.036
581 Baltz, A.G., Munschauer, M., Schwanhäusser, B., Vasile, A., Murakawa, Y., Schueler, M.,
582 Youngs, N., Penfold-Brown, D., Drew, K., Milek, M., Wyler, E., Bonneau, R., Selbach, M.,
583 Dieterich, C., Landthaler, M., 2012. The mRNA-bound proteome and its global occupancy
584 profile on protein-coding transcripts. Mol. Cell 46, 674–690.
585 doi:10.1016/j.molcel.2012.05.021
586 Battich, N., Stoeger, T., Pelkmans, L., 2015. Control of Transcript Variability in Single
587 Mammalian Cells. Cell 163, 1596–1610. doi:10.1016/j.cell.2015.11.018
588 Cooper, T.A., Wan, L., Dreyfuss, G., 2009. RNA and Disease. Cell 136, 777–793.
589 doi:10.1016/j.cell.2009.02.011
590 Corcoran, D.L., Georgiev, S., Mukherjee, N., Gottwein, E., Skalsky, R.L., Keene, J.D., Ohler,
591 U., 2011. PARalyzer: definition of RNA binding sites from PAR-CLIP short-read sequence
592 data. Genome Biol. 12, R79. doi:10.1186/gb-2011-12-8-r79
593 Fan, X.C., Steitz, J.A., 1998. HNS, a nuclear-cytoplasmic shuttling sequence in HuR. Proc. Natl.
594 Acad. Sci. U.S.A. 95, 15293–15298.
595 Farina, K.L., Hüttelmaier, S., Musunuru, K., Darnell, R., Singer, R.H., 2003. Two ZBP1 KH
596 domains facilitate β-actin mRNA localization, granule formation, and cytoskeletal
597 attachment. The Journal of Cell Biology 160, 77–87. doi:10.1083/jcb.200206003
598 Fredericks, A.M., Cygan, K.J., Brown, B.A., Fairbrother, W.G., 2015. RNA-Binding Proteins:
599 Splicing Factors and Disease. Biomolecules 5, 893–909. doi:10.3390/biom5020893
600 Friedersdorf, M.B., Keene, J.D., 2014. Advancing the functional utility of PAR-CLIP by
601 quantifying background binding to mRNAs and lncRNAs. Genome Biol. 15, R2.
602 doi:10.1186/gb-2014-15-1-r2
603 Garzia, A., Jafarnejad, S.M., Meyer, C., Chapat, C., Gogakos, T., Morozov, P., Amiri, M.,

604 Shapiro, M., Molina, H., Tuschl, T., Sonenberg, N., 2017a. The E3 ubiquitin ligase and
605 RNA-binding protein ZNF598 orchestrates ribosome quality control of premature
606 polyadenylated mRNAs. Nat Commun 8, 16056. doi:10.1038/ncomms16056
607 Garzia, A., Meyer, C., Morozov, P., Sajek, M., Tuschl, T., 2017b. Optimization of PAR-CLIP
608 for transcriptome-wide identification of binding sites of RNA-binding proteins. Methods
609 118-119, 24–40. doi:10.1016/j.ymeth.2016.10.007
610 Gerstberger, S., Hafner, M., Tuschl, T., 2014. A census of human RNA-binding proteins. Nature
611 Reviews Genetics 15, 829–845. doi:10.1038/nrg3813
612 Gruber, A.J., Schmidt, R., Gruber, A.R., Martin, G., Ghosh, S., Belmadani, M., Keller, W.,
613 Zavolan, M., 2016. A comprehensive analysis of 3' end sequencing data sets reveals novel
614 polyadenylation signals and the repressive role of heterogeneous ribonucleoprotein C on
615 cleavage and polyadenylation. Genome Res. 26, 1145–1159. doi:10.1101/gr.202432.115
616 Guillaumet-Adkins, A., Rodríguez-Esteban, G., Mereu, E., Mendez-Lago, M., Jaitin, D.A.,
617 Villanueva, A., Vidal, A., Martinez-Marti, A., Felip, E., Vivancos, A., Keren-Shaul, H.,
618 Heath, S., Gut, M., Amit, I., Gut, I., Heyn, H., 2017. Single-cell transcriptome conservation
619 in cryopreserved cells and tissues. Genome Biol. 18, 45. doi:10.1186/s13059-017-1171-9
620 Hafner, M., Landthaler, M., Burger, L., Khorshid, M., Hausser, J., Berninger, P., Rothballer, A.,
621 Ascano, M., Jungkamp, A.-C., Munschauer, M., Ulrich, A., Wardle, G.S., Dewell, S.,
622 Zavolan, M., Tuschl, T., 2010. Transcriptome-wide identification of RNA-binding protein
623 and microRNA target sites by PAR-CLIP. Cell 141, 129–141.
624 doi:10.1016/j.cell.2010.03.009
625 Hubstenberger, A., Courel, M., Bénard, M., Souquere, S., Ernoult-Lange, M., Chouaib, R., Yi,
626 Z., Morlot, J.-B., Munier, A., Fradet, M., Daunesse, M., Bertrand, E., Pierron, G.,
627 Mozziconacci, J., Kress, M., Weil, D., 2017. P-Body Purification Reveals the Condensation
628 of Repressed mRNA Regulons. Mol. Cell 68, 144–157.e5. doi:10.1016/j.molcel.2017.09.003
629 Jankowsky, E., Harris, M.E., 2015. Specificity and nonspecificity in RNA-protein interactions.
630 Nat. Rev. Mol. Cell Biol. 16, 533–544. doi:10.1038/nrm4032
631 Jønson, L., Vikesaa, J., Krogh, A., Nielsen, L.K., Hansen, T.V., Borup, R., Johnsen, A.H.,
632 Christiansen, J., Nielsen, F.C., 2007. Molecular composition of IMP1 ribonucleoprotein
633 granules. Mol. Cell Proteomics 6, 798–811. doi:10.1074/mcp.M600346-MCP200
634 Keene, J.D., 2007. RNA regulons: coordination of post-transcriptional events. Nature Reviews
635 Genetics 8, 533–543. doi:10.1038/nrg2111
636 Kishore, S., Jaskiewicz, L., Burger, L., Hausser, J., Khorshid, M., Zavolan, M., 2011. A
637 quantitative analysis of CLIP methods for identifying binding sites of RNA-binding proteins.
638 Nat. Methods 8, 559–564. doi:10.1038/nmeth.1608
639 Koutmou, K.S., Schuller, A.P., Brunelle, J.L., Radhakrishnan, A., Djuranovic, S., Green, R.,
640 2015. Ribosomes slide on lysine-encoding homopolymeric A stretches. Elife 4, 446.
641 doi:10.7554/eLife.05534
642 König, J., Zarnack, K., Rot, G., Curk, T., Kayikci, M., Zupan, B., Turner, D.J., Luscombe, N.M.,
643 Ule, J., 2010. iCLIP reveals the function of hnRNP particles in splicing at individual
644 nucleotide resolution. Nat. Struct. Mol. Biol. 17, 909–915. doi:10.1038/nsmb.1838
645 Lebedeva, S., Jens, M., Theil, K., Schwanhäusser, B., Selbach, M., Landthaler, M., Rajewsky,
646 N., 2011. Transcriptome-wide analysis of regulatory interactions of the RNA-binding protein
647 HuR. Mol. Cell 43, 340–352. doi:10.1016/j.molcel.2011.06.008
648 Li, B., Dewey, C.N., 2011. RSEM: accurate transcript quantification from RNA-Seq data with or
649 without a reference genome. BMC Bioinformatics 12, 323. doi:10.1186/1471-2105-12-323

650 Maatz, H., Jens, M., Liss, M., Schafer, S., Heinig, M., Kirchner, M., Adami, E., Rintisch, C.,
651 Dauksaite, V., Radke, M.H., Selbach, M., Barton, P.J.R., Cook, S.A., Rajewsky, N.,
652 Gotthardt, M., Landthaler, M., Hubner, N., 2014. RNA-binding protein RBM20 represses
653 splicing to orchestrate cardiac pre-mRNA processing. J. Clin. Invest. 124, 3419–3430.
654 doi:10.1172/JCI74523
655 Mansfield, K.D., Keene, J.D., 2012. Neuron-specific ELAV/Hu proteins suppress HuR mRNA
656 during neuronal differentiation by alternative polyadenylation. Nucleic Acids Res. 40, 2734–
657 2746. doi:10.1093/nar/gkr1114
658 Marçais, G., Kingsford, C., 2011. A fast, lock-free approach for efficient parallel counting of
659 occurrences of k-mers. Bioinformatics 27, 764–770. doi:10.1093/bioinformatics/btr011
660 Martin, G., Gruber, A.R., Keller, W., Zavolan, M., 2012. Genome-wide analysis of pre-mRNA
661 3“ end processing reveals a decisive role of human cleavage factor I in the regulation of 3”
662 UTR length. Cell Rep 1, 753–763. doi:10.1016/j.celrep.2012.05.003
663 Mesarovic, M.D., Sreenath, S.N., Keene, J.D., 2004. Search for organising principles:
664 understanding in systems biology. Syst Biol (Stevenage) 1, 19–27.
665 Moore, M.J., 2005. From birth to death: the complex lives of eukaryotic mRNAs. Science 309,
666 1514–1518. doi:10.1126/science.1111443
667 Mukherjee, N., Calviello, L., Hirsekorn, A., de Pretis, S., Pelizzola, M., Ohler, U., 2017.
668 Integrative classification of human coding and noncoding genes through RNA metabolism
669 profiles. Nat. Struct. Mol. Biol. 24, 86–96. doi:10.1038/nsmb.3325
670 Mukherjee, N., Corcoran, D.L., Nusbaum, J.D., Reid, D.W., Georgiev, S., Hafner, M., Ascano,
671 M., Tuschl, T., Ohler, U., Keene, J.D., 2011. Integrative regulatory mapping indicates that
672 the RNA-binding protein HuR couples pre-mRNA processing and mRNA stability. Mol.
673 Cell 43, 327–339. doi:10.1016/j.molcel.2011.06.007
674 Mukherjee, N., Jacobs, N.C., Hafner, M., Kennington, E.A., Nusbaum, J.D., Tuschl, T.,
675 Blackshear, P.J., Ohler, U., 2014. Global target mRNA specification and regulation by the
676 RNA-binding protein ZFP36. Genome Biol. 15, R12. doi:10.1186/gb-2014-15-1-r12
677 Munteanu, A., Mukherjee, N., Ohler, U., 2018. SSMART: Sequence-structure motif
678 identification for RNA-binding proteins. bioRxiv 287953. doi:10.1101/287953
679 Nielsen, F.C., Nielsen, J., Christiansen, J., 2001. A family of IGF-II mRNA binding proteins
680 (IMP) involved in RNA trafficking. Scand. J. Clin. Lab. Invest. Suppl. 234, 93–99.
681 Pandit, S., Zhou, Y., Shiue, L., Coutinho-Mansfield, G., Li, H., Qiu, J., Huang, J., Yeo, G.W.,
682 Ares, M., Fu, X.-D., 2013. Genome-wide analysis reveals SR protein cooperation and
683 competition in regulated splicing. Mol. Cell 50, 223–235. doi:10.1016/j.molcel.2013.03.001
684 Pullmann, R., Kim, H.H., Abdelmohsen, K., Lal, A., Martindale, J.L., Yang, X., Gorospe, M.,
685 2007. Analysis of turnover and translation regulatory RNA-binding protein expression
686 through binding to cognate mRNAs. Mol. Cell. Biol. 27, 6265–6278.
687 doi:10.1128/MCB.00500-07
688 Sheth, U., Parker, R., 2003. Decapping and decay of messenger RNA occur in cytoplasmic
689 processing bodies. Science 300, 805–808. doi:10.1126/science.1082320
690 Sundararaman, B., Zhan, L., Blue, S.M., Stanton, R., Elkins, K., Olson, S., Wei, X., Van
691 Nostrand, E.L., Pratt, G.A., Huelga, S.C., Smalec, B.M., Wang, X., Hong, E.L., Davidson,
692 J.M., Lécuyer, E., Graveley, B.R., Yeo, G.W., 2016. Resources for the Comprehensive
693 Discovery of Functional RNA Elements. Mol. Cell 61, 903–913.
694 doi:10.1016/j.molcel.2016.02.012
695 Tenenbaum, S.A., Carson, C.C., Lager, P.J., Keene, J.D., 2000. Identifying mRNA subsets in

messenger ribonucleoprotein complexes by using cDNA arrays. Proc. Natl. Acad. Sci. U.S.A. 97, 14085–14090. doi:10.1073/pnas.97.26.14085

Ule, J., Jensen, K.B., Ruggiu, M., Mele, A., Ule, A., Darnell, R.B., 2003. CLIP identifies Nova-regulated RNA networks in the brain. Science 302, 1212–1215. doi:10.1126/science.1090095

Van Nostrand, E.L., Pratt, G.A., Shishkin, A.A., Gelboin-Burkhart, C., Fang, M.Y., Sundararaman, B., Blue, S.M., Nguyen, T.B., Surka, C., Elkins, K., Stanton, R., Rigo, F., Guttman, M., Yeo, G.W., 2016. Robust transcriptome-wide discovery of RNA-binding protein binding sites with enhanced CLIP (eCLIP). Nat. Methods 13, 508–514. doi:10.1038/nmeth.3810

Wilusz, J., Feig, D.I., Shenk, T., 1988. The C proteins of heterogeneous nuclear ribonucleoprotein complexes interact with RNA sequences downstream of polyadenylation cleavage sites. Mol. Cell. Biol. 8, 4477–4483.

Zhang, C., Frias, M.A., Mele, A., Ruggiu, M., Eom, T., Marney, C.B., Wang, H., Licatalosi, D.D., Fak, J.J., Darnell, R.B., 2010. Integrative modeling defines the Nova splicing-regulatory network and its combinatorial controls. Science 329, 439–443. doi:10.1126/science.1191150

Zhao, J., Ohsumi, T.K., Kung, J.T., Ogawa, Y., Grau, D.J., Sarma, K., Song, J.J., Kingston, R.E., Borowsky, M., Lee, J.T., 2010. Genome-wide identification of polycomb-associated RNAs by RIP-seq. Mol. Cell 40, 939–953. doi:10.1016/j.molcel.2010.12.011

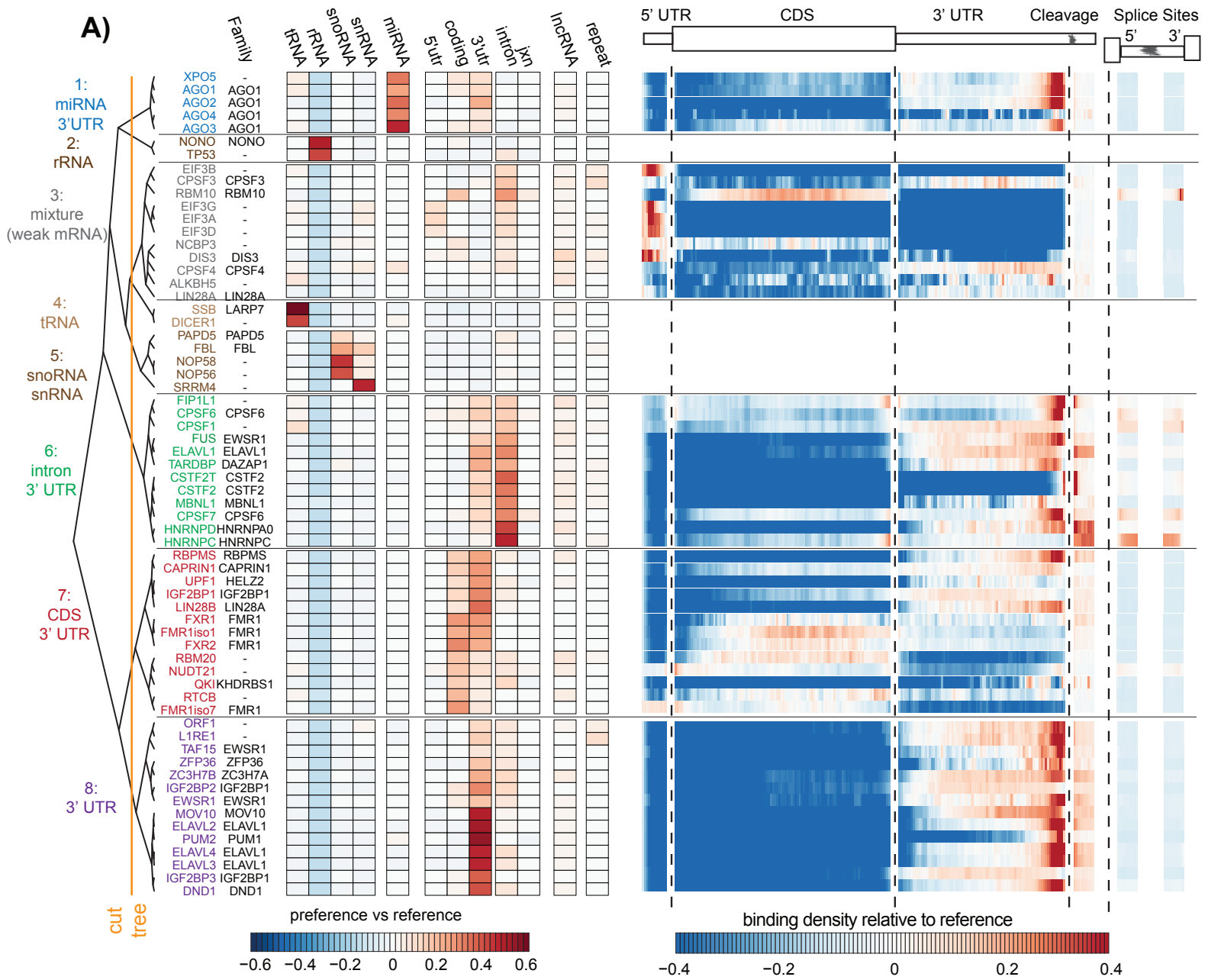
A)
Family
tRNA
rRNA
snoRNA
snRNA
miRNA
5'utr
coding
3'utr
intron
jxn
lncRNA
repeat
5' UTR
CDS
3' UTR
Cleavage
Splice Sites
5'
3'
1: miRNA 3'UTR
2: rRNA
3: mixture (weak mRNA)
4: tRNA
5: snoRNA snRNA
6: intron 3' UTR
7: CDS 3' UTR
8: 3' UTR
cut tree
XPO5 -
AGO1 AGO1
AGO2 AGO1
AGO4 AGO1
AGO3 AGO1
NONO NONO
TP53 -
EIF3B -
CPSF3 CPSF3
RBM10 RBM10
EIF3G -
EIF3A -
EIF3D -
NCBP3 -
DIS3 DIS3
CPSF4 CPSF4
ALKBH5 -
LIN28A LIN28A
SSB LARP7
DICER1 -
PAPD5 PAPD5
FBL FBL
NOP58 -
NOP56 -
SRRM4 -
FIP1L1 -
CPSF6 CPSF6
CPSF1 -
FUS EWSR1
ELAVL1 ELAVL1
TARDBP DAZAP1
CSTF2T CSTF2
CSTF2 CSTF2
MBNL1 MBNL1
CPSF7 CPSF6
HNRNPD HNRNPA0
HNRNPC HNRNPC
RBPMS RBPMS
CAPRIN1 CAPRIN1
UPF1 HELZ2
IGF2BP1 IGF2BP1
LIN28B LIN28A
FXR1 FMR1
FMR1iso1 FMR1
FXR2 FMR1
RBM20 -
NUDT21 -
QKI KHDRBS1
RTCB -
FMR1iso7 FMR1
ORF1 -
L1RE1 -
TAF15 EWSR1
ZFP36 ZFP36
ZC3H7B ZC3H7A
IGF2BP2 IGF2BP1
EWSR1 EWSR1
MOV10 MOV10
ELAVL2 ELAVL1
PUM2 PUM1
ELAVL4 ELAVL1
ELAVL3 ELAVL1
IGF2BP3 IGF2BP1
DND1 DND1
preference vs reference
−0.6 −0.4 −0.2 0 0.2 0.4 0.6
binding density relative to reference
−0.4 −0.2 0 0.2 0.4

A)

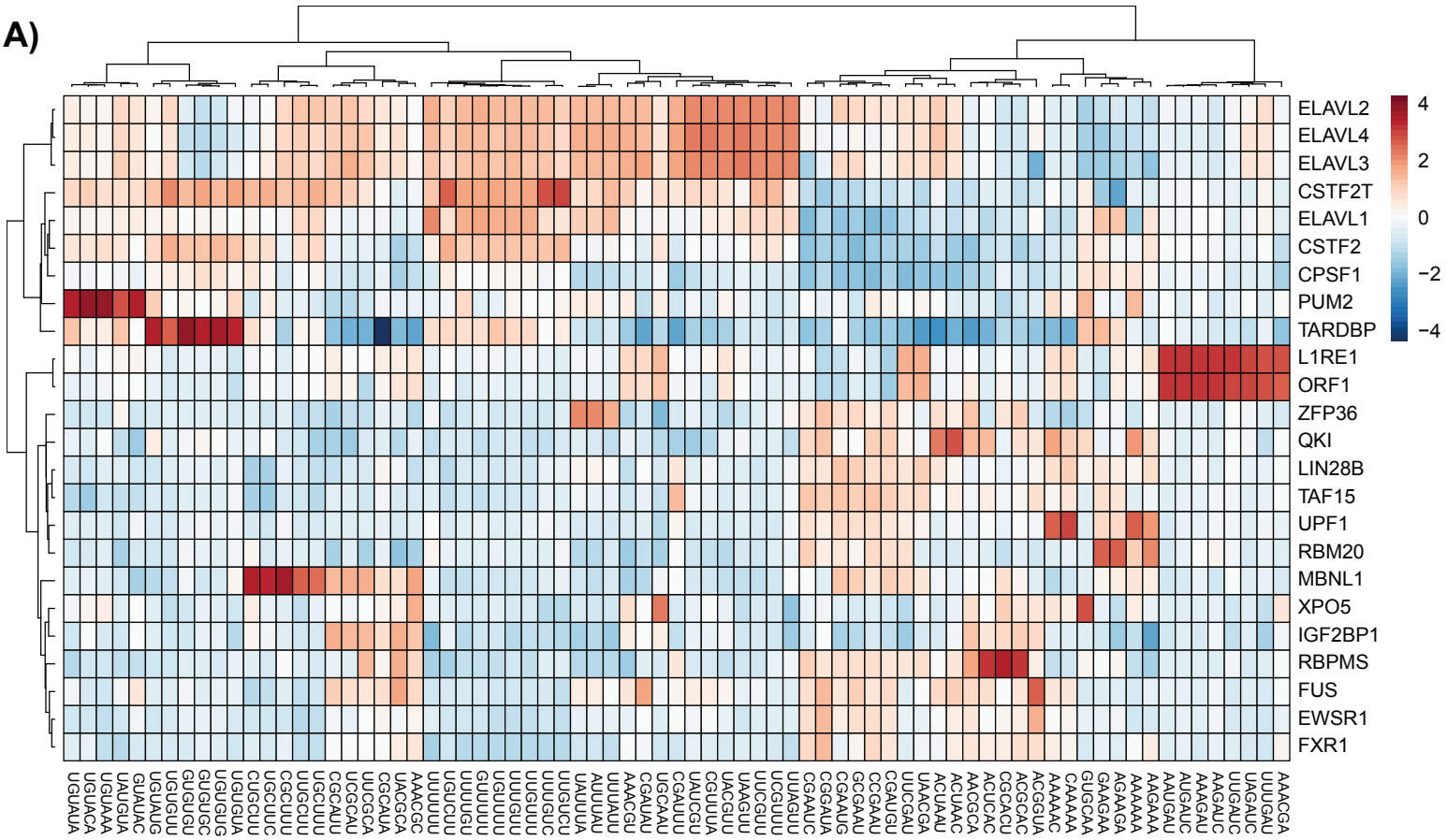
ELAVL2
ELAVL4
ELAVL3
CSTF2T
ELAVL1
CSTF2
CPSF1
PUM2
TARDBP
L1RE1
ORF1
ZFP36
QKI
LIN28B
TAF15
UPF1
RBM20
MBNL1
XPO5
IGF2BP1
RBPMS
FUS
EWSR1
FXR1
4
2
0
−2
−4
UGUAUA
UGUACA
UGUAAA
UAUGUA
GUAUAC
UGUAUG
UGUGUU
GUGUGU
GUGUGC
UGUGUG
UGUGUA
CUGCUU
UGCUUC
CGCUUU
UGCUUU
UGCUUU
CGCAUU
UCGCAU
UUCGCA
CGCAUA
UACGCA
AAACGC
UUUUUU
UGUCUU
UUUUGU
GUUUUU
UGUUUU
UUUGUU
UUUGUC
UUUGUC
UAUUUA
AUUUAU
UUUAUU
AAACGU
CGAUAU
UGCAAU
CGAUUU
UAUCGU
CGUUUA
UACGUU
UAAGUU
UUCGUU
UCGUUU
UUAGUU
CGAAUC
CGGAUA
CGAAUG
GCGAAU
CCGAAU
CGAUGU
UUCGAU
UAACGA
ACUAAU
ACUAAC
AACGCA
ACUCAC
CGCACU
ACGCAC
ACGGUA
AAAAAC
CAAAAA
GUGCAA
GAAGAA
AGAAGA
AAAAAA
AAGAAA
AAUGAU
AUGAUC
AAGAUC
UUGAUC
UAGAUC
UUUGAU
AAACGA

A)

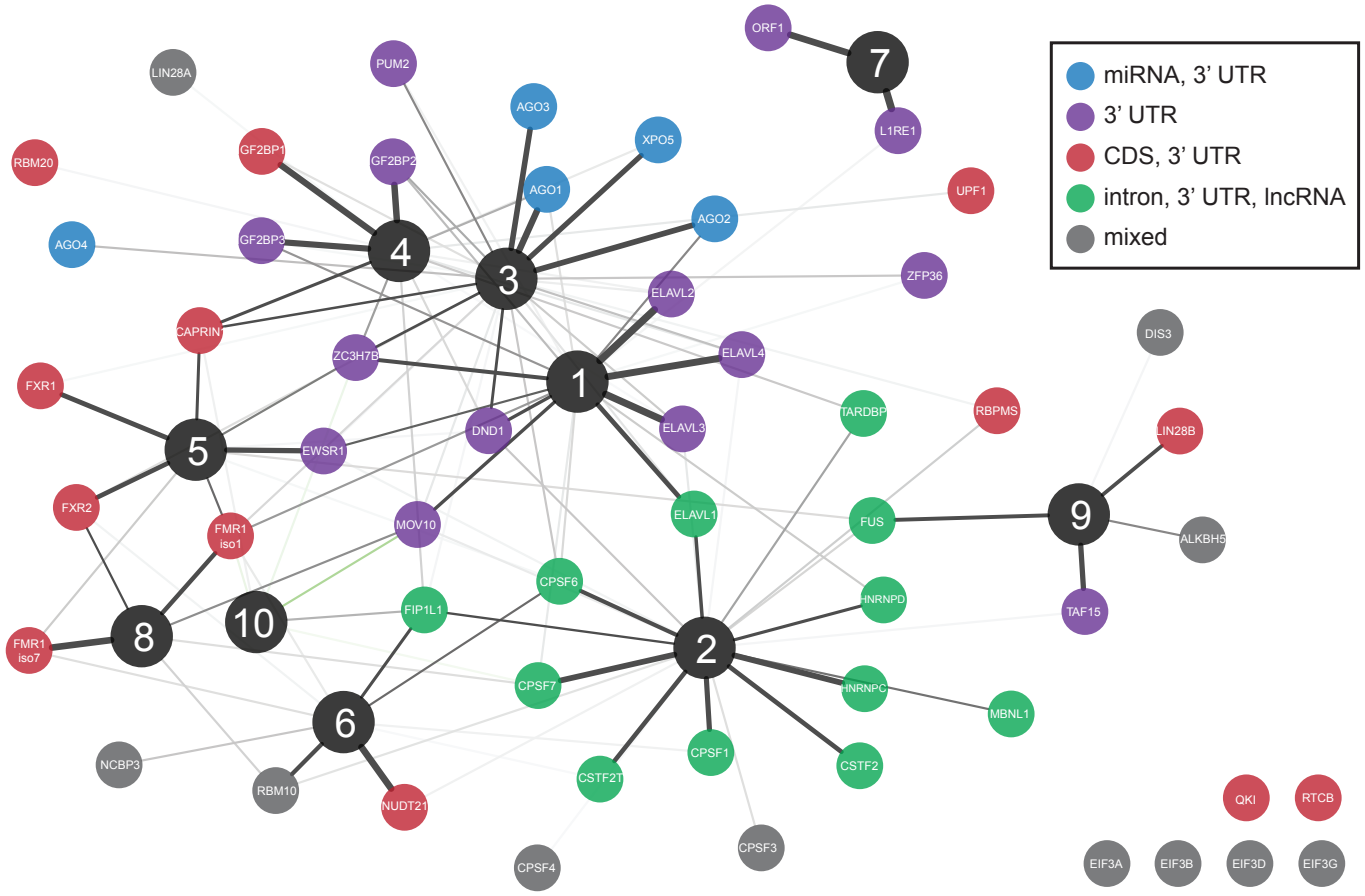
miRNA, 3' UTR
3' UTR
CDS, 3' UTR
intron, 3' UTR, lncRNA
mixed
1
2
3
4
5
6
7
8
9
10
ORF1
L1RE1
LIN28A
PUM2
AGO3
XPO5
RBM20
GF2BP1
GF2BP2
AGO1
UPF1
AGO2
AGO4
GF2BP3
ZFP36
ELAVL2
CAPRIN1
ZC3H7B
ELAVL4
DIS3
FXR1
TARDBP
RBPMS
DND1
ELAVL3
LIN28B
EWSR1
FXR2
ELAVL1
FUS
FMR1 iso1
MOV10
ALKBH5
CPSF6
HNRNPD
TAF15
FIP1L1
FMR1 iso7
CPSF7
HNRNPC
MBNL1
NCBP3
CPSF1
CSTF2
CSTF2T
RBM10
NUDT21
QKI
RTCB
CPSF3
CPSF4
EIF3A
EIF3B
EIF3D
EIF3G

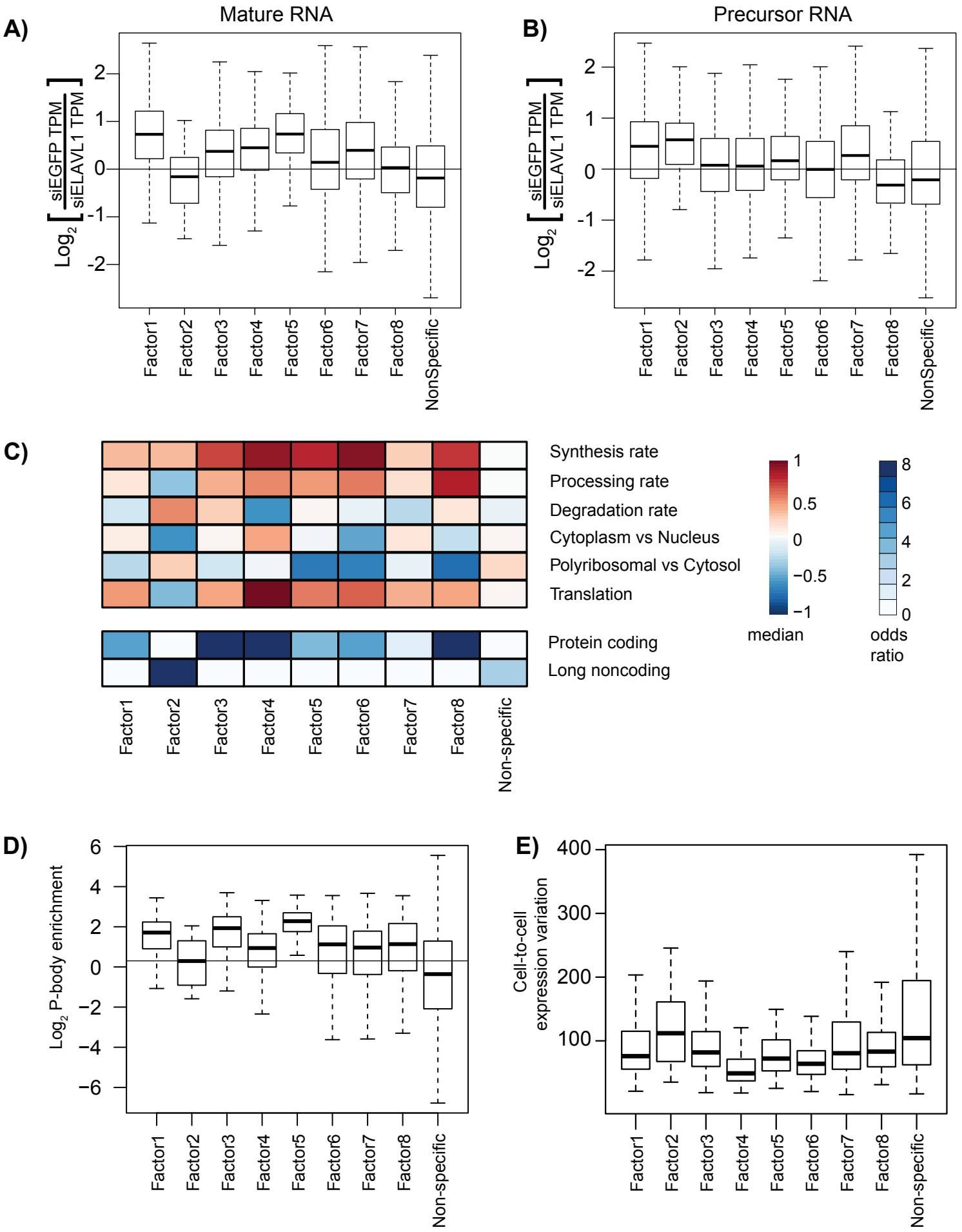
A)
Mature RNA
Log2 [siEGFP TPM / siELAVL1 TPM]
2
1
0
-1
-2
Factor1
Factor2
Factor3
Factor4
Factor5
Factor6
Factor7
Factor8
NonSpecific
B)
Precursor RNA
Log2 [siEGFP TPM / siELAVL1 TPM]
2
1
0
-1
-2
Factor1
Factor2
Factor3
Factor4
Factor5
Factor6
Factor7
Factor8
NonSpecific
C)
Synthesis rate
Processing rate
Degradation rate
Cytoplasm vs Nucleus
Polyribosomal vs Cytosol
Translation
Protein coding
Long noncoding
Factor1
Factor2
Factor3
Factor4
Factor5
Factor6
Factor7
Factor8
Non-specific
1
0.5
0
−0.5
−1
median
8
6
4
2
0
odds ratio
D)
Log2 P-body enrichment
6
4
2
0
−2
−4
−6
Factor1
Factor2
Factor3
Factor4
Factor5
Factor6
Factor7
Factor8
Non-specific
E)
Cell-to-cell expression variation
400
300
200
100
Factor1
Factor2
Factor3
Factor4
Factor5
Factor6
Factor7
Factor8
Non-specific